Structural Study of Zirconium Phosphate−Nafion Hybrid Membranes for High-Temperature Proton Exchange Membrane Fuel Cell Applications

D. Truffier-Boutry,[†,‡] A. De Geyer,[†] L. Guetaz,[§] O. Diat,[†] and G. Gebel*[,†]

Structure et Propriétés d'Architectures Moléculaires, UMR 5819 SPrAM (CEA-CNRS-UJF), 38054 Grenoble cedex 9, France, and Laboratoire Composants pour PEM, LITEN-DTH, CEA-Grenoble; 17 avenue des Martyrs, 38054 Grenoble cedex 9, France

Received March 19, 2007; Revised Manuscript Received July 20, 2007

ABSTRACT: The structure of inorganic fillers dispersed in proton exchange membranes for fuel cell (PEMFC) was investigated by X-ray scattering and electron microscopy. The hybrid membranes have been obtained by an in situ precipitation of zirconium phosphate (α-ZrP) particles within a perfluorosulfonated ionomer membrane (Nafion). An extended angular range in the scattering experiments was covered in order to analyze simultaneously the crystalline structure of the particles, their shape and their size. At wide angles, the scattering peaks characteristic of the presence of α-ZrP have been observed and the width analysis of the scattering peak corresponding to the stacking of α-ZrP layers suggests a packing of 10−13 α-ZrP layers. The small angle spectra reveal that the structure of the membrane is not modified by the introduction of inorganic species and the excess of scattering intensity due to inorganic particles is well reproduced by the form factor of oblate ellipsoids, with a semimajor axis length of about 280 Å and a semiminor axis length of about 35 Å. These results are confirmed by high-resolution scanning electron microscopy.

Introduction

The Nafion membrane, a perfluorosulfonated copolymer commercialized by DuPont de Nemours & Co.[1] remains actually the benchmark polymer for the proton exchange membrane for fuel cell (PEMFC) in terms of protonic conduction and mechanical, chemical, and electrochemical stabilities.[2] In automotive applications, PEMFCs will operate over a wide range of temperatures from subzero temperatures in winter conditions up to temperatures as high as possible. High temperatures are necessary in order to improve the ionic conductivity, catalytic and heat exchange processes. The loss of performance under these extreme conditions is usually due to problems of water management in a first step and to the membrane−electrode assembly degradation under cycling conditions in a second step. As a consequence, many researches focus on these aspects.

At subzero temperatures, the membrane partially dehydrates[3] and the water freezes in the active layer of the membrane-electrode assembly, damaging the electrode structure.[4,5] At high temperatures, the membrane also dehydrates due to water evaporation reducing significantly the ionic conductivity. As a consequence, the operating conditions in automotive application lead to a large series of membrane swelling-deswelling cycles inducing a mechanical fatigue and the membrane failure. Different issues are investigated in order to maintain a high PEMFC performance in these extreme conditions. A first commonly explored issue is to simplify the problem of water management using nonvolatile, thermally and electrochemically stable protonic conductors in the absence of water. Polybenzimidazole doped with phosphoric acid were extensively studied.[6] Ionic liquid[7] appears also as potentially interesting for instance trapped in an inorganic skeleton to prevent its leaching of the membrane.[8] However, most of these systems present significant proton conductivity only at elevated temperatures. The other commonly explored issue consists in the introduction of hydrophilic inorganic and conducting species within the membrane to trap water molecules, promote a Grotthus type vehicular mechanism at high temperatures, and enhance the mechanical properties by acting as fillers.[9]

Different inorganic fillers such as SiO_2 particles,[10] clays,[11,12] and submicrometer particles of phosphatoantimonic acid[13] were incorporated in organic membranes either by direct sol−gel synthesis within the membranes[10] or by dispersing the inorganic particles in the ionomer solution and preparing membranes by solution-casting.[12] The α-zirconium phosphate (α-ZrP) is known for its outstanding chemical stability and Nafion−α-ZrP is one of the first examples of organic−inorganic composite membranes designed for a use as an ion exchange membrane operating in harsh conditions such as chlor-alkali electrolysis.[14] Twenty years later, these hybrid membranes were considered as promising materials for a use in fuel cells. First, α-ZrP is a Bronsted acid with the ability to donate protons, increasing the mobility of protons on its surface and thus the conductivity. Second, hydrophilic α-ZrP particles are expected to trap water molecules and enhance Nafion conductivity at low relative humidity. Finally, the synthesis procedure is compatible with the chemical and physical limits of the polymer membrane.[15]

α-ZrP particles were then incorporated in many different organic membranes like Nafion,[16−18] or sulfonated aromatic polymers[19−22] and nonconducting polymer matrix like PVDF.[23] Numerous data on the ionic conductivity, the water uptake, or the thermal stability have been published including the study in fuel cell conditions.[24] However, no prototype able to operate at temperatures larger than 80 °C was yet unveiled using this technology. Moreover, while it is commonly believed that the ionic transport and swelling properties of the membranes are

† Structure et Propriétés d'Architectures Moléculaires, UMR 5819 SPrAM (CEA-CNRS-UJF).
§ Laboratoire Composants pour PEM, LITEN-DTH, CEA-Grenoble.
* Corresponding author.
‡ Presently at LEPMI, INPG Grenoble.

10.1021/ma0706576 CCC: $37.00
Published on Web 10/11/2007

strongly related to their microstructure, no complete structural studies on hybrid membranes have been published in order to determine the shape, the size, and the distribution of the particles within the polymer matrix. Tchicaya et al.[20] and Costamagna et al.[25] observed a scattering peak in the X-ray diffraction pattern attributed to the stacking confirming the layered structure of the α-ZrP within organic membranes whereas Bauer et al.[16] did not observed it. The most suitable tool to extract structural information is the small-angle scattering technique covering the largest angular range as possible.[26] Small-angle X-ray scattering (SAXS) was combined with wide-angle scattering (WAXS) and scanning electron microscopy (SEM) was used to determine for the first time the geometry of the zirconium phosphate particles, their size and their distribution within the Nafion membrane.

Experimental Section

(1) Preparation of Organic/Inorganic Hybrid Membranes. First, 4 cm^2 samples of Nafion 115 membranes from du Pont de Nemours (125 μm thick membranes) were first cleaned in a 1 M aqueous solution of nitric acid during 2 h at 80 °C. The excess of acid was then removed by rinsing twice the membranes in deionized (DI) water during 2 h at 80 °C. The membranes were dried during one night at 50 °C in an oven under vacuum and then, weighed in order to determine the initial weight (W_i). The second step consisted in the incorporation of the inorganic species in the organic membrane by using the method described in the literature.[15] The cation exchange membrane was soaked in an 1 M aqueous solution of zirconium dichloride oxide $ZrOCl_2 8H_2O$ from Alfa Aesar during 4 h at 80 °C leading to an exchange of the protons of the Nafion membrane by the Zr cations from the solution. The membrane was then rinsed in deionized (DI) water during 2 h at room temperature to remove the excess of zirconium species at the surface of the membrane. The weight increase due to the exchange process was determined after drying the samples overnight at 50 °C under vacuum.

Zirconium phosphate (ZrP) was then precipitated in situ in the membrane by soaking it in a 1 M aqueous solution of phosphoric acid during 2 h at 80 °C. The ionomer membrane was soaked in a 1.5 M sulfuric acid during 2 h at 80 °C for acidification. The rinsing procedure was again applied to remove the excess of acid. Membranes were then dried one night at 50 °C under vacuum and weighed in order to obtain the final weight (W_f).

The weight percent of the inorganic species incorporated in the organic membrane was determined according to the following equation:

$$W\,[\mathrm{ZrP}]\ (\mathrm{wt}\ \%) = 100 \times (W_f - W_i)/W_i \qquad (1)$$

(2) Membrane Characterization. (a) Scanning Electron Microscopy (SEM). The samples were cryo-fractured in liquid nitrogen and observed in the cross-section by SEM.

The distribution of the inorganic fillers has been observed with a SEM 840A from JEOL equipped with an energy dispersive X-ray spectroscopy (EDX) detector on samples covered with carbon. Two different accelerating voltages with a current of 3 nA were used (20 and 40 kV) in order to differentiate the contribution of zirconium and phosphorus atoms.

The visualization of the inorganic objects was carried out with a SEM-FEG (field emission gun) LEO 1530 which allows analysis with lower accelerating voltage (5 kV) without any deposit on the samples.

(b) Wide-Angle and Small-Angle X-ray Scattering (SAXS—WAXS). The structural organization has been studied by small- and wide-angle X-ray scattering (SAXS−WAXS) with a homemade apparatus using a Cu Kα radiation ($\lambda = 1.5418$ $Å^{-1}$) source generated by a rotating anode. Three sample to detector distances varying from 0.1 to 3 m were used to cover an angular range from $q = 0.01$ to 3 $Å^{-1}$ where q is the momentum transfer ($q = (4\pi(\sin\theta)/\lambda)$) and 2θ is the total scattering angle. Two pieces of membrane (5 × 5 mm) were superposed and were placed in a brass cell between 2 Kapton sheets. Usual corrections for background subtraction and intensity normalization using Lupolen as standard were applied.

Additional experiments were performed to increase the angular range: (i) at wide angles (from 3 to 7 $Å^{-1}$) using a X'pert diffractometer from 7 to 150° at 0.04°/s in the reflected radiation mode, with a Co Kα radiation ($\lambda = 1.78897$ $Å^{-1}$) source operating at 50 kV and 35 mA; (ii) at ultralow angles (from 10^{-4} to 10^{-3} $Å^{-1}$) using the Bonse & Hart camera on the ID2 beamline (ESRF-Grenoble).[27]

Results and Discussion

Both the $ZrOCl_2$ solution concentration and the duration of immersion at 80 °C have been optimized to ensure a complete exchange of the membrane. The first step of the α-ZrP incorporation within the ionomer membrane is often described as an exchange process of the protons by Zr^{4+} cations during the immersion of the membrane in the zirconyl chloride solution.[25] However, two different hypotheses have been also published: (i) Tchicaya et al.[28] concluded from EXAFS experiments that the zirconium species are introduced as $[Zr_4(OH)_8(H_2O)_{16}]^{8+}$ macro cations in sulfonated poly(arylene)ether membranes; (ii) the zirconium species could be present in Nafion as ZrO^{2+}.[29] The calculated weight increase assuming ion exchange with $[Zr_4(OH)_8(H_2O)_{16}]^{8+}$, $[ZrO]^{2+}$, and $[Zr]^{4+}$ on a membrane equivalent weight of 1100 g/equiv are respectively 8.96%, 4.87%, and 2.07%. The experimental weight increase after immersion in the zirconyl choride solution was found to be around 4.5% w/w which suggests an exchange with ZrO^{2+} ions. However, the dissolution of $ZrOCl_2$ produces a large quantity of acidic moieties and a complete exchange of the membranes by Zr cations cannot be insured. In addition, the ion exchange process can be hindered in the presence of large Zr cations like $[Zr_4(OH)_8(H_2O)_{16}]^{8+}$. Therefore, a lower weight increase consecutive to a partial ion exchange can be obtained, but the ion exchange by Zr^{4+} species can be excluded.

After reaction by immersion in the 1 M H_3PO_4 solution, the α-ZrP content in the organic membrane is 14.5% w/w. The concentration of the phosphoric acid solution is also an important parameter. A 1 M concentration was chosen as a good compromise since both 5 and 0.1 M solutions lead to lower weight increases. Tchicaya et al.[28] have observed that using a solution with a concentration higher than 5 M reduces considerably the precipitation of α-ZrP probably because of an inverse exchange of the Zr cations by the protons of the phosphoric acid and a partial solubility of α-ZrP in concentrated H_3PO_4. The experimental weight increase due α-ZrP ($Zr(HPO_4)_2H_2O$) precipitation is close to the calculated value assuming an exchange by $[ZrO]^{2+}$ cations in the first step ($W_{\alpha-Zr} = 12.64\%$). At the contrary, the hypothesis of a partial exchange by $[Zr_4(OH)_8(H_2O)_{16}]^{8+}$ cations after immersion in the zirconyl choride solution appears highly improbable since the maximum weight increase after precipitation of zirconium phosphate should be 6.9%w/w which is significantly smaller than the experimental value. Therefore, combining the measurements after exchange and precipitation, we can conclude that the zirconium cations are inserted in the membrane as $[ZrO]^{2+}$.

In Figure 1 are presented the zirconium concentration profiles determined by scanning electron microscopy after precipitation of α-ZrP. The concentration profiles reveal that the average quantity of α-ZrP is relatively constant along the membrane thickness. However, the dispersion of the measurement around the average value is pretty large suggesting a noncompletely homogeneous distribution on a sub-micrometer scale (typically

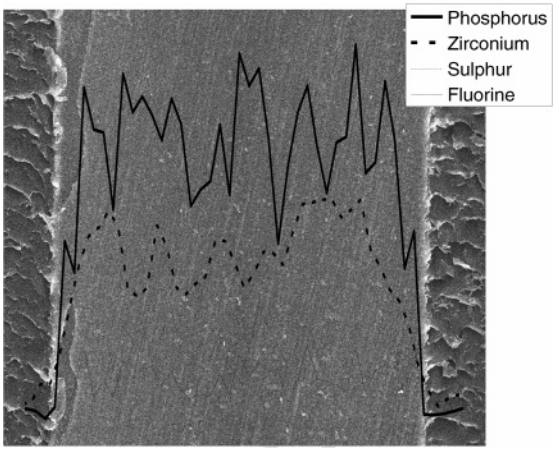

Figure 1. SEM micrograph of a Nafion/ZrP hybrid membrane with phosphorus, zirconium, sulfur and fluorine concentration profiles along the membrane thickness.

the SEM EDX resolution). Because of the overlap between the energy peaks of zirconium and phosphorus, it was not possible to accurately determine the Zr/P ratio.

Structural Study. From a structural point of view, each layer of α-ZrP consists of planes of zirconium atoms bridged through phosphate groups which alternate above and below the metal atom planes.[30,31] Three of the phosphate oxygen bonds to three different zirconium atoms. The fourth one bears the hydrogen and points toward an adjacent layer or at the surface of the stacking of several layers, inducing the surface acidity of the inorganic particle. The layers are arranged relative to each other in such a way to form six sided zeolitic type cavities interconnected by entrances with sizes large enough to allow a spherical ion of a diameter of 2.63 Å to diffuse into the cavities. Therefore, a water molecule can reside in the center of each cavity. Moreover, −POH groups are involved in inter- and intra-planar bonds because half of these groups are believed to form hydrogen bonds with phosphate oxygen atoms in an adjacent layer[32] and the others are thought to be hydrogen bonded to the water molecules.[33] Therefore, they were trapped in the inorganic particle, even at high temperature since Slade et al.[34] have showed that the α-ZrP structure remains unchanged until 220 °C. From the conduction point of view, Alberti et al.[35,36] stated that the greater part of the internal transport occurs in the parallel direction to the layers and he has proved that the intercalated molecules (alkali ions or water molecules) are mobile inside the α-ZrP. Therefore, they contribute to ionic conduction through diffusion within the cavities but 10^4 times weaker than the surface one because of a free space limitation between layers forbidding the Grotthus type conduction of hydronium ions.

(a) Scattering Results. The structure of Nafion−ZrP hybrid membranes has been investigated by small- and wide-angle X-ray scattering covering the widest angular range as possible (from 0.0001 to 7 $Å^{-1}$) using different configurations and spectrometers. These experiments were carried out in order to access to the internal structure of the particles, to their size and shape and finally to extract some information on their spatial distribution. A piece of Nafion membrane which has been submitted to the same swelling and acidification procedures was also studied as reference (Figure 2A). The structure of the reference and Nafion/zirconium phosphate hybrid material appears to be very different at both wide and small angles.

In these small and wide angle ranges of momentum transfers (Figure 2A), the 3 characteristic peaks of the Nafion membrane

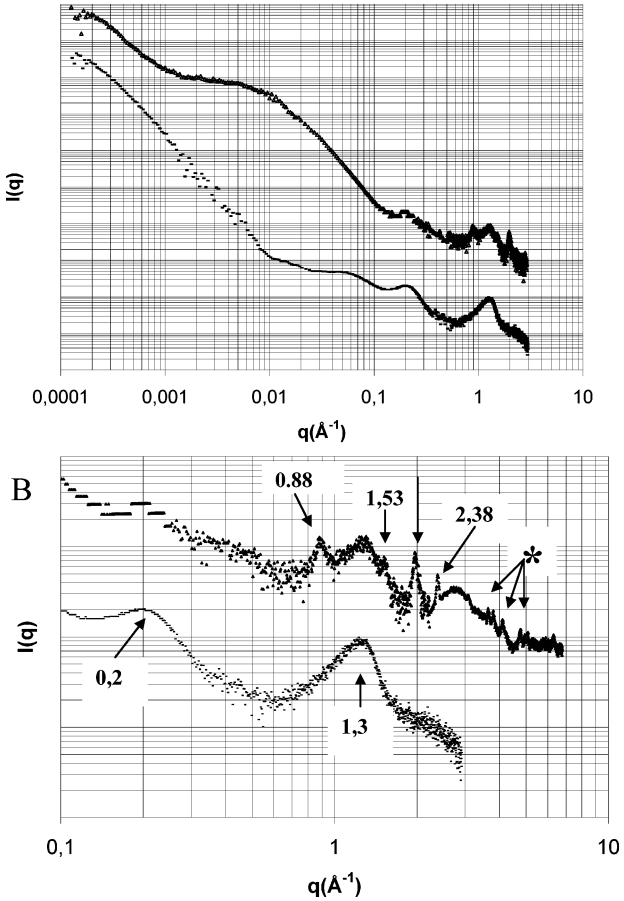

Figure 2. (A) SAXS−WAXS curves obtained with Nafion reference (bottom), and Nafion/ZrP hybrid membrane (top). An offset by a factor ten was applied to the hybrid membrane spectrum for clarity. (B) Zoom on the wide angle scattering part of the Nafion/ZrP spectrum.

are clearly observed: (i) the broad signal at about 1.3 $Å^{-1}$ characteristic of the distance between polymer segments and composed of an intense amorphous halo and a small crystalline peak;[37] (ii) the ionomer peak at about 0.2 $Å^{-1}$ commonly attributed to the distance between ionic domains;[26,38] (iii) a very broad maximum at 0.06 $Å^{-1}$ corresponding to the long range period between polymer crystallites.[37,38]

When α-ZrP is incorporated into Nafion, additional well-defined peaks appear at large angles (Figure 2B). According to the literature, when α-ZrP is precipitated outside a membrane from an aqueous solution, several reflections are highlighted at q (momentum transfer) of about 0.82, 1.39, 1.41, 1.76, and 2.38 $Å^{-1}$.[39] At larger q values, several other peaks are observed by XRD attributed to distances inside the layers: Zr−O bonds (at about $q \sim 3$ $Å^{-1}$), P−OH bonds (at about $q \sim 3.92$ $Å^{-1}$), and P−O bonds (at about $q \sim 4.16$ $Å^{-1}$).[31] Possible O−O bonds could be also observed from $q \sim 2.05$ to 2.26 $Å^{-1}$. When α-ZrP is incorporated in the membrane, a few of these reflections are recovered (Figure 2B). At large angles, peaks attributed to Zr−O and P−O(H) are clearly observed (∗ in Figure 2), and at lower q, four sharp peaks appear α. They are located at $q = 0.88$, 1.5, 1.97, and 2.38 $Å^{-1}$ instead of 0.82, 1.41, 1.76, and 2.39 $Å^{-1}$, respectively, as mentioned by Clearfield for bulk α-ZrP. The peak expected at 1.39 $Å^{-1}$ is probably hidden by the intense and broad scattering of the Nafion amorphous and crystalline matrix α. Important information (Figure 2) is the observation of the correlation peak at 0.88 $Å^{-1}$ characteristic of the stacking of several ZrP layers. This interlayer distance (7.14 Å) slightly differs from the one found by Clearfield, which is probably due

to an effect of confinement on the stacking formation inside the Nafion membrane. This peak is pretty large compared to the other crystalline peaks suggesting that the packing along this direction does not extend over large distances. The size of the inorganic crystallites along the stacking direction has been estimated, based on the width of this interlayer peak diffraction, by using the Scherrer equation (2).

$$B = K\lambda/L(\cos\theta) \tag{2}$$

where B is the half-width height of the stacking peak, K is a constant equal to 0.9λ, and L is the average particle size.

The peak width analysis has been performed on the experimental curve subtracted by the reference curve. The average size of the particles along the perpendicular direction to the α-ZrP layers is about 95 Å. With an interlayer distance of 7.14 Å, the average number of layers can then be estimated to be about 13 layers per crystallite.

At low angles, an excess of scattering intensity is clearly seen in Figure 2 which can be attributed to the inorganic particles. The high level of scattered intensity and the low angular position of this signal compared to the ionomer peak position suggest the existence of very large particles. Moreover, the absence of correlation peak at low angles indicates that the particles are likely to be widely separated (no aggregation) without any significant correlation in position and orientation. The intensity was adjusted using the form factor of ellipsoids of revolution:[40]

$$\frac{I(q)}{\phi_{Zr}} = \Delta\rho^2\, V\, P(q)^2$$

$$\text{with } P(q) = \int_0^{\pi/2} F_1[q, r(R,\epsilon,\alpha)](\sin\alpha)\, d\alpha \tag{3}$$

where $r(R,\epsilon,\alpha) = R(\sin^2\alpha + \epsilon^2\cos^2\alpha)^{1/2,}$ ϵ is the eccentricity, V is the volume of the particles, ϕ_{Zr} their volume fraction, $\Delta\rho$ the contrast factor, and

$$F_1(q,R) = \frac{3(\sin(qR) - qR\cos(qR))}{(qR)^3} \quad \text{and } V = 4\pi\epsilon\, R^3/3 \tag{4}$$

The eccentricity is defined as the ratio of two main axes where the axis in the denominator is the one which rotates around the fixed axis. Depending on its value, spherical ($\epsilon = 1$), prolate ellipsoids ($\epsilon > 1$) or oblate ellipsoids ($\epsilon \ll 1$) can be evaluated. In other words, the same function can be used to check different shapes from rodlike ($\epsilon \gg 1$) or platelet-like ($\epsilon \ll 1$) objects. The data can be well reproduced by the form factor of oblate ellipsoids (Figure 3). A pretty large polydispersity in the particle size is expected at least because the precipitation reaction begins at the membrane surface and propagates inside the membrane when immersed in the phosphoric acid solution. The main effect of such a polydispersity (Gaussian or log−normal radius distribution) is a smoothing effect of the large angle oscillations of the form factor without modifying its shape in the low angle region used for the fitting procedure. It is always possible to fit any data assuming a spherical or elongated shape but at the expense of the introduction of a specific size distribution (and consequently an infinite number of adjusting parameters). For example, the data can be quite well reproduced using a spherical shape and a bimodal radius distribution. However, there is no objective reason to introduce such hypotheses. In addition, the oblate ellipsoid shape was confirmed by the electron microscopy study presented below.

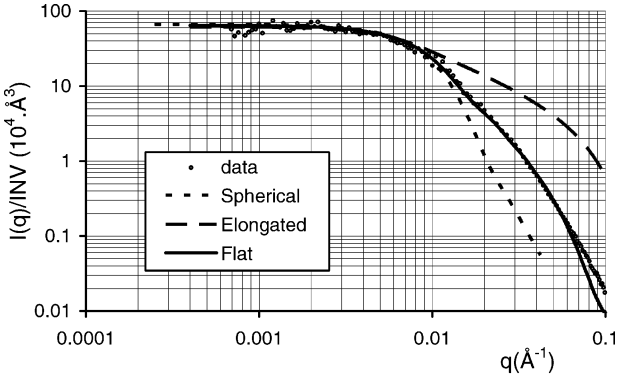

Figure 3. SAXS intensity normalized by the scattering invariant (o) and best adjustments with the form factors of spherical, prolate, and oblate ellipsoids.

For the analysis of scattering experiments, it is very useful to fit the level of intensity in addition to the shape of the curve to validate the model. It requires the estimation of the contrast factor, $\Delta\rho$, which depends on both the atomic composition and the density of each phase. The contrast factor for Nafion/ZrP hybrid membranes can be easily calculated in the case of completely dry membranes. For membranes equilibrated at room temperature, the membrane will contain a significant quantity of water molecules and their distribution between the two phases is unknown. Therefore, we have chosen to normalize the data by the scattering invariant in order to avoid any supplementary assumption. For a two-phase system, the scattering invariant is experimentally determined as the:

$$INV = \int_0^\infty I(q)q^2\, dq = 2\pi^2(\Delta\rho)^2\phi_{Zr}(1-\phi_{Zr}) \tag{5}$$

The experimental invariant is calculated by q integration of the data according to the first part of eq 5. Combining eq 3 and the second part of eq 5, one obtains :

$$\frac{I(q)}{INV} = \frac{V}{2\pi^2(1-\phi_{Zr})}P(q)^2 \tag{6}$$

The two-phase approximation could be considered as crude for a multiphase system but it is justified by the fact that the signal due α-ZrP particles is located at q values 10 times lower compared to structural signature of Nafion (Figure 2). Therefore, Nafion can be considered as a homogeneous matrix at this scale which will be further confirmed by the comparison of the fit obtained with invariant normalized and absolute intensities. On the basis of this assumption, the scattering contribution of Nafion can be subtracted from the hybrid membrane spectrum (Figure 3) since the Nafion microstructure does not appear to be influenced as revealed by the behavior at q values larger than 0.1 Å^{-1} and lower than 0.001 Å^{-1} (the ionomer peak and the upturn at very low angles are not modified).

The best fit as presented in Figure 3 was obtained with 280 and 35 Å as semimajor and semiminor axis lengths, respectively. It is worth noting that both the shape and the dimensions of the particles extracted from this analysis are average values. The quality of the adjustment will not benefit from the introduction of polydispersity, and thus no reliable information can be obtained on this parameter. However, it is likely that the α-ZrP particles are not perfect and regular objects. The fit with the form factor of oblate ellipsoid reveals that the particles can be characterized by two main characteristic dimensions (56 nm wide, 7 nm thick) but the actual structure should be seen as in

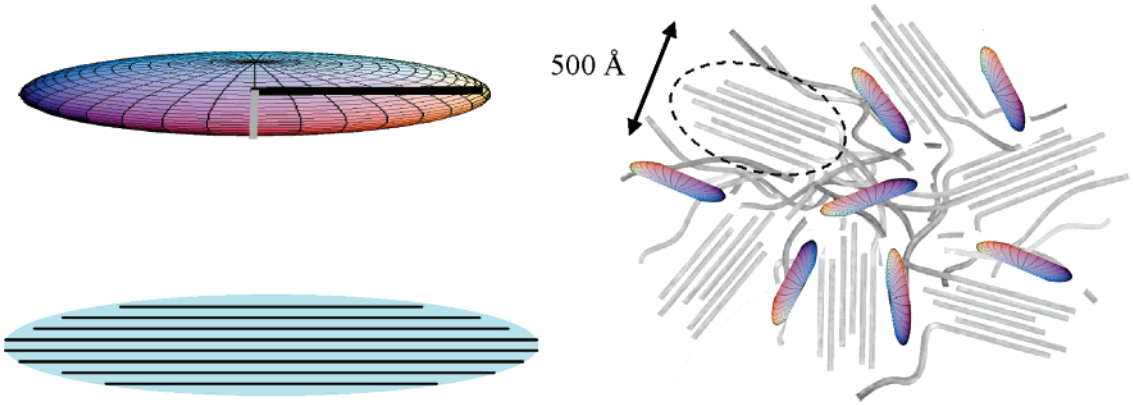

Figure 4. Oblate ellipsoid with a semimajor axis length (in black) of about 280 Å and with a semiminor axis length (in gray) of about 35 Å (left top). Stacking of layers in the oblate ellipsoid inorganic object (left bottom) and most probable localization of the inorganic objects within the Nafion membrane structure (right). The dashed line highlights a bundle of elongated polymer aggregates.

between an oblate ellipsoid and a flat particle. The absolute scale of scattered intensities is also very well reproduced. The contrast factor was calculated using the densities found in the literature ($d_{\alpha-ZrP} = 2.72$ and $d_{Nafion} = 2.1$ g/cm^3). The SAXS experiments were carried out with membranes equilibrated at room humidity. The quality of the intensity adjustment without taking into account the sorption of water molecules suggests that an almost equal distribution of the water molecules between Nafion and α-ZrP phases at room temperature and humidity which is not really surprising since both phases are considered as highly hydrophilic.

With an interlayer distance of about 7.14 Å, it can be estimated that the α-ZrP crystal is constituted of 10 layers which is in good agreement with the value extracted from the width of the scattering peak using the Scherrer equation. A disk-like shape corresponds to the prediction from calculation on the α-ZrP precipitated outside a membrane by Clearfield[31] where hexagonal platelets have been found. The inorganic particles are expected to be templated by the Nafion internal microstructure due to the in situ synthesis process. This structure is still subject to debate but the recent ribbon-like polymer particle model appears as the most suitable model to describe the main structural features and transport properties of these membranes.[41,42] The local structure is formed by polymer ribbons with the ionic groups at the water−polymer interface. The cross-section was estimated to be 1 nm thick and 7 nm wide. These ribbons are locally oriented and form bundles which are randomly distributed in the absence of mechanical deformation. The typical size of these bundles which was estimated between 50 and 100 nm from both USAXS and atomic force microscopy experiments.[42] The size of the ionic domains is estimated between 1 and 5 nm from SAXS and SANS data depending on the membrane water content and the chosen structural model.[26] Therefore, the inorganic particles are at least 1 order of magnitude larger than the size of the ionic domains in Nafion. As a consequence, these inorganic objects should not be located in the ionic pathways of the Nafion but they are distributed at rather larger scale which is likely to be between the bundles of polymer chain aggregates (Figure 4). The present result suggests a competition between the α-ZrP particle formation and the ion exchange process of Zr cations by the protons of the acidic solution. Both the penetration of protons in the membrane and the exchange process seems very fast compared to the diffusion of the zirconium cations which accumulate within the inter-bundle zones and form α-ZrP particles. It can then be expected that changing parameters such as the concentration of the acidic solution or the reaction temperature will act differently on the competing processes and will lead to different size and distribution of the inorganic species within Nafion. In the present paper, we have limited the SAXS investigation to the sample presenting the largest weight increase and a crystalline structure for ZrP particles. The in situ synthesis is very sensitive to the experimental procedure. Reproducible weight increases and WAXS spectra can be obtained using exactly the same preparation process. The size and distribution of ZrP determined in this work should be representative to the hydrid membrane structure when the particles are crystallized. The analysis of samples containing less α-ZrP is more complex. Indeed, the size of the α-ZrP particles is closer to the characteristic dimensions of Nafion and, in the presence of nonnegligible cross-terms, it would be no more valid to consider additive contributions of the polymer and particles. In this case, it would be more suitable to use small-angle neutron scattering experiments and contrast variation to match the polymer matrix contribution and see only inorganic particles. The quantity of α-ZrP introduced within Nafion can be increased by reproducing several times the optimized exchange-precipitation procedure on the same sample. However, it is highly probable that a bimodal or more complex size distribution would be obtained which would be difficult to analyze.

(c) Visualization by SEM. SEM-FEG observations have been conducted on the hybrid membrane which has been previously cryo-fractured in order to visualize the structure along the membrane thickness. The inorganic particles dispersed in the polymer matrix appear as platelets without any preferential orientation and widely spaced (Figure 5). Some fluffy domains appears on the pictures which can be attributed either to some α-ZrP species highly dispersed in the polymer matrix or more likely to α-ZrP particles embedded below the surface. This observation is in agreement with the results deduced from the SAXS analysis. A second sample has been prepared by calcination of the organic matrix at 600 °C in the presence of oxygen. In this case, the particles are more clearly visible but a sintering effect due to the thermal treatment at elevated temperature induces a growth of the objects which thus appear significantly larger than in the direct observation of the membrane.

Conclusions

The shape and the size of zirconium phosphate prepared in situ in Nafion membrane have been determined using a

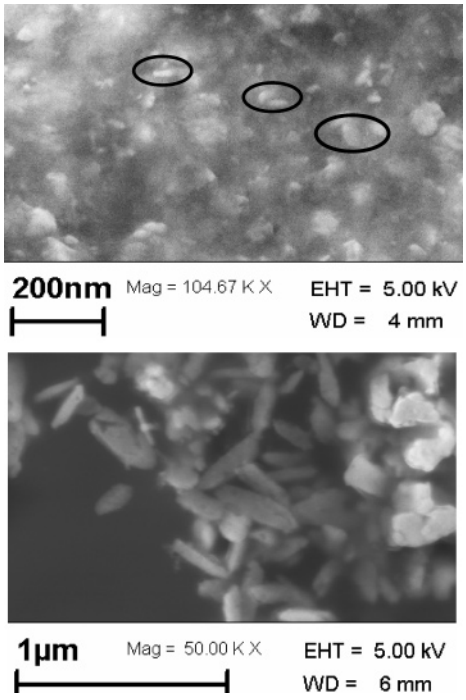

Figure 5. SEM micrograph of Nafion/ZrP4h: freeze fracture (top) and residue after Nafion calcination (bottom).

combination of WAXS, SAXS and SEM-FEG. The inorganic particles are homogeneously distributed along the membrane cross section. They appear as 56 nm wide platelets with a thickness of 7 nm corresponding to the stacking of about 10−13 layers of α-ZrP. These large dimensions suggest that the synthesis does not occur within the ionic domains but in the inter bundle areas where the spatial arrangement of the perfluorinated ribbon should be less compact. As a consequence, these particles present some ion conducting properties but probably do not promote the proton conduction on a local scale. However, they could help for water retention at elevated temperature by acting as nanotanks dispersed in the perfluorinated matrix with an inter distance of 50−100 nm. On a structural point of view, this technique of in situ growth of inorganic particles followed by the calcinations of the organic matrix could have been used to get negative image of the internal structure of ionomer membranes which can be easily observed by electron microscopy. However, it has been shown that the growth of the inorganic particles is restricted to the zones where large objects can be obtained and the calcinations procedure induce a sintering of the particles probably due to surface activation.

Acknowledgment. The authors acknowledge the CEA-DRT-DPSE for financial support through the NTE transverse program and Jean-Jacques Allegraud for his work in the overall study and especially the SEM concentration profile determination. We would like to thank T. Narayanan (ID2 ESRF beamline) for allowing us some test beam-time on the USAXS instruments. We also thank the reviewers for their fruitful comments.

References and Notes

(1) *Perfluorinated Ionomer Membranes*; Eisenberg, A., Yeager, H. L., Eds.; 1982.
(2) *Handbook of fuel cells: fundamentals, technology, applications*; Vielstich, W., Lamm, A., Gasteiger, H., Eds.; John Wiley: New York, 2004.
(3) Pinéri, M.; Volino, F.; Escoubes, M. *J. Polym. Sci., Part B: Polym. Phys.* **1985**, *23*, 2009.
(4) Yan, Q.; Toghiani, H.; Lee, Y.-W.; Liang, K.; Causey, H. *J. Power Sources* **2006**, *160*, 1242.
(5) Pinéri, M.; Gebel, G.; Diat, O.; Davies, R. J. Submitted to *J. Power Sources*.
(6) Wang, J. T.; Savinell, R. F.; Wainright, J.; Litt, M.; Yu, H. *Electrochim. Acta* **1996**, *41*, 193.
(7) Bonhôte, P.; Dias, A.-P.; Papageorgiou, N.; Kalyanasundaram, K.; Grätzel, M. *Inorg. Chem.* **1996**, *35*, 1168.
(8) Néouze, M-A.; Le Bideau, J.; Leroux, F.; Vioux, A. *Chem. Commun.* **2005**, 1082.
(9) Bauer, F.; Willert-Porada, M. *J. Power Sources* **2005**, *145*, 101.
(10) Vallé, K.; Belleville, P.; Pereira, F.; Sanchez, C. *Nat. Mater.* **2006**, *5*, 107.
(11) Thomassin, J.-M.; Pagnoulle, C.; Caldarella, G.; Germain, A.; Jérôme, R. *J. Membr. Sci.* **2006**, *270*, 50.
(12) Bebin, P.; Caravanier, M.; Galiano, H. *J. Membr. Sci.* **2006**, *278*, 35.
(13) Baradie, B.; Poinsignon, C.; Sanchez, J.-Y.; Piffard, Y.; Vitter, G.; Bestaoui, N.; Foscallo, D.; Denoyelle, A.; Delabouglise, D.; Vaujany, M. *J. Power Sources* **1998**, *74*, 8.
(14) Murayama, N.; Sakagami, T.; Fukuda, M. French patent, 7609347, 1976.
(15) Grot, W. G.; Rajendran, G. United States Patent 5,919,583, 1999.
(16) Bauer, F.; Willert-Porada, M. *J. Membr. Sci.* **2004**, *233*, 141.
(17) Yang, C.; Srinivasan, S.; Arico, A. S.; Creti, P.; Baglio, V.; Antonucci, V. *Electrochem. Solid-State Lett.* **2001**, *4*, A31.
(18) Tiwari, S. K.; Agarwal, Y. K.; Nema, S. K. *Ind. J. Eng. Mater. Sci.* **2000**, *7*, 35.
(19) Bonnet, B.; Jones, D. J.; Rozière, J.; Tchicaya, L.; Alberti, G.; Casciola, M.; Massinelli, B.; Bauer, B.; Peraio, A.; Ramunni, E. *J. New Mat. Electrochem. Syst.* **2000**, *3*, 87.
(20) Tchicaya-Bouckary, L.; Jones, D. J.; Rozière, J. *Fuel Cells* **2002**, *2*, 40.
(21) Hill, M. L.; Kim, Y. S.; Einsla, B. R.; McGrath, J. E. *J. Membr. Sci.* **2006**, *283*, 102.
(22) Woo, M. H.; Kwon, O.; Choi, S. H.; Hong, M. Z.; Ha, H.-W.; Kim, K. *Electrochim. Acta* **2006**, *51*, 6051.
(23) Casciola, M.; Donnadio, A.; Pica, M.; Valentini, V.; Piaggio, P. *Macromol. Symp.* **2005**, *230*, 95.
(24) Bauer, F.; Willert-Porada, M. *Fuel Cells* **2006**, *6*, 261.
(25) Costamagna, P.; Yang, C.; Bocarsly, A. B.; Srinivasan, S. *Electrochim. Acta* **2002**, *47*, 1023.
(26) Gebel, G.; Diat, O. *Fuel Cells: Fundam. Syst.* **2005**, *5*, 261.
(27) Narayanan, T.; Diat, O.; Bösecke, P. *Nucl. Instrum. Methods Phys. Res. A* **2001**, *467−468*, 1005.
(28) Tchicaya-Bouckary, L. Ph.D. Thesis, Université de Montpellier II, Montpellier, France, 2000.
(29) Kerres, J. A. *Fuel Cells* **2005**, *5*, 230.
(30) Amphlett, C. B.; McDonald, L. A.; Redman, M. J. *J. Inorg. Chem.* **1958**, *6*, 220.
(31) Clearfield, A.; Smith, G. D. *Inorg. Chem.* **1969**, *8*, 431.
(32) Clearfield, A.; Stynes, J. A. *J. Inorg. Nucl. Chem.* **1963**, *26*, 117.
(33) Alberti, G.; Torracca, E. *J. Inorg. Nucl. Chem.* **1968**, *30*, 317.
(34) Slade, R. C. T.; Knowles, J. A.; Jones, D. J.; Rozière, J. *Solid State Ionics* **1997**, *96*, 9.
(35) Alberti, G.; Casciola, M.; Costantino, U.; Levi, G.; Ricciardi, G. *J. Inorg. Chem.* **1978**, *40*, 533.
(36) Alberti, G.; Casciola, M.; Costantino, U.; Leonardi, M. *Solid State Ionics* **1984**, *14*, 289.
(37) Fujimura, M.; Hashimoto, T.; Kawai, H. *Macromolecules* **1981**, *14*, 1309.
(38) Gierke, T. D.; Munn, G. E.; Wilson, F. C. *J. Polym. Sci.: Polym. Phys. Ed.* **1981**, *19*, 1687.
(39) Alberti, G.; Costantino, U.; Alluli, S.; Massucci, M. A. *J. Inorg. Nucl. Chem.* **1975**, *37*, 1779.
(40) Pedersen, J. S. *Adv. Colloid Interface Sci.* **1997**, *70*, 171.
(41) Rubatat, L.; Rollet, A.-L.; Gebel, G.; Diat, O. *Macromolecules* **2002**, *35*, 4050.
(42) Rubatat, L.; Gebel, G.; Diat, O. *Macromolecules* **2004**, *37*, 7772.

MA0706576